



HAL
open science

Sustainability, transfer and containment properties of concrete subject to delayed ettringite formation (DEF)

Arthur Pichelin, Myriam Carcasses, Franck Cassagnabère, Stéphane Multon,
G. Nahas

► To cite this version:

Arthur Pichelin, Myriam Carcasses, Franck Cassagnabère, Stéphane Multon, G. Nahas. Sustainability, transfer and containment properties of concrete subject to delayed ettringite formation (DEF). *Cement and Concrete Composites*, 2020, 113, pp.103738. 10.1016/j.cemconcomp.2020.103738 . hal-02995601

HAL Id: hal-02995601

<https://insa-toulouse.hal.science/hal-02995601v1>

Submitted on 22 Aug 2022

HAL is a multi-disciplinary open access archive for the deposit and dissemination of scientific research documents, whether they are published or not. The documents may come from teaching and research institutions in France or abroad, or from public or private research centers.

L'archive ouverte pluridisciplinaire **HAL**, est destinée au dépôt et à la diffusion de documents scientifiques de niveau recherche, publiés ou non, émanant des établissements d'enseignement et de recherche français ou étrangers, des laboratoires publics ou privés.



Distributed under a Creative Commons Attribution - NonCommercial 4.0 International License

1 Sustainability, transfer and containment properties of concrete subject to Delayed 2 Ettringite Formation (DEF).

3 A. Pichelin^(a,b), M. Carcassès^(a), F. Cassagnabère^(a), S. Multon^(a), G. Nahas^(b)

4
5 (a) *Laboratoire Matériaux et Durabilité des Constructions (LMDC), Toulouse, France.*

6 (b) *Institut de Radioprotection et de Sûreté Nucléaire (IRSN), Fontenay-aux-Roses, France.*

7 **Abstract**

8 This work used numerous experimental techniques to evaluate the physicochemical and
9 mechanical modifications of concrete damaged by swelling due to internal sulfate attack. The
10 first objective was to determine property sensitive to DEF (delayed ettringite formation) and
11 able to detect it before apparent cracking. The second objective was to quantify the evolution
12 of the properties that impact the containment property and the sustainability of concrete after
13 expansion and damage. It was found that gas permeability, electrical resistivity and static
14 moduli results were the most promising techniques to detect DEF during the latency period.
15 The loss of containment appears for damage lower than 20%.

16 **Keywords:** Delayed Ettringite Formation (DEF); Sustainability indicators; Internal Sulfate
17 Attack (ISA); Swelling; Nuclear structure; containment property.

18 **1. Introduction**

19 Internal Sulfate Attack (ISA) can be due to the formation of delayed ettringite (DEF) in
20 cementitious material, after concrete hardening and without external sulfate supply. Many
21 engineering structures are susceptible to develop these pathologies. This reaction requires the
22 presence of three main factors: high sulfate and aluminate contents, water, and a rise in
23 temperature at young age and/or later. The reaction mechanisms of DEF are complex but
24 Brunetaud has proposed a global mechanism, described in four phases, grouping many
25 theories [1]. Several parameters have an influence on the development of DEF, and can be
26 divided into two groups: those related to the formulation of concrete and those related to the
27 environment. Concerning the formulation parameters, the expansion generated is strongly
28 dependent on the nature of the binder, in particular on the sulfate, aluminate and alkali
29 contents [2, 3]. The amount of added water is also influential. It modifies the porosity and
30 therefore the ionic transfer [2, 4]. In addition, the nature and size of aggregates are important;
31 it has been shown that the use of small siliceous aggregates significantly increases the kinetics
32 and the swelling potential of DEF [5, 6]. As far as the environmental conditions are

33 concerned, DEF requires a minimum of 90% relative humidity and a rise in temperature to
34 above 65°C once in its history [7]. Expansion increases with the water content of concrete [8].
35 In terms of temperature, results from the literature show a combined influence of the maximal
36 temperature and the duration when the temperature is higher than about 65°C [9]. The
37 evaluation of DEF damage in nuclear power plants represents an important economic and
38 societal challenge. The main consequences of DEF are expansion and cracks. They affect the
39 physicochemical and mechanical properties of the concrete. Cracks lead to an increase of
40 transfer properties and a decrease of mechanical properties and may lead to a loss of
41 containment, which is harmful for nuclear power plants. Massive elements can be particularly
42 sensitive to DEF due to the risk of temperature increase at young age caused by the heat
43 production during cement hydration [10]. It therefore becomes necessary to propose a
44 measurement method to assess the state of degradation of the concrete generated by DEF in
45 such elements. Few data can be found in the literature on the evolution of the
46 physicochemical and mechanical properties of concrete according to the degree of
47 advancement of DEF. The present study had two objectives: first, to find a very sensitive test
48 allowing DEF to be detected before cracking can be observed visually and, second, to
49 evaluate the evolution of the properties that impact the containment and also the sustainability
50 of concrete affected by usual concrete pathologies such as carbonation, corrosion, etc. A test
51 protocol to accelerate DEF development was carried out and provided a good representation
52 of the reality on site [11]. A large number of samples were used to characterize the impact of
53 DEF on concrete properties at different levels of expansion. Chemical tests were performed to
54 observe the initiation and the presence of DEF, while physical and mechanical tests evaluated
55 the impact of DEF on mechanical and transfer properties.

56 **2. Experiments**

57 **2.1. Materials**

58 *2.1.1. Components*

59 In this study, two cements and two types of aggregates were used. The choice of cements
60 focused on a CEMI and a CEMII, the main characteristics of which are summarized in Table
61 1. The aggregates used were based on silica or limestone according to the formulations. These
62 two cements have been used in previous studies and show a high swelling potential in the case
63 of DEF, in particular because of their high sulfate, alkali and aluminate contents [8, 11].

64

65

Mass content (%)	CEM I 52.5 N	CEMII/A-LL 42.5 R
SiO ₂	19.3	19.7
CaO	63.2	63.5
Al ₂ O ₃	5.3	4.6
Fe ₂ O ₃	2.6	3.2
K ₂ O	0.94	1.36
Na ₂ O	0.08	0.11
SO ₃	3.5	2.7
Total	94.92	95,17

Table 1: Cement composition

2.1.2. Mix designs

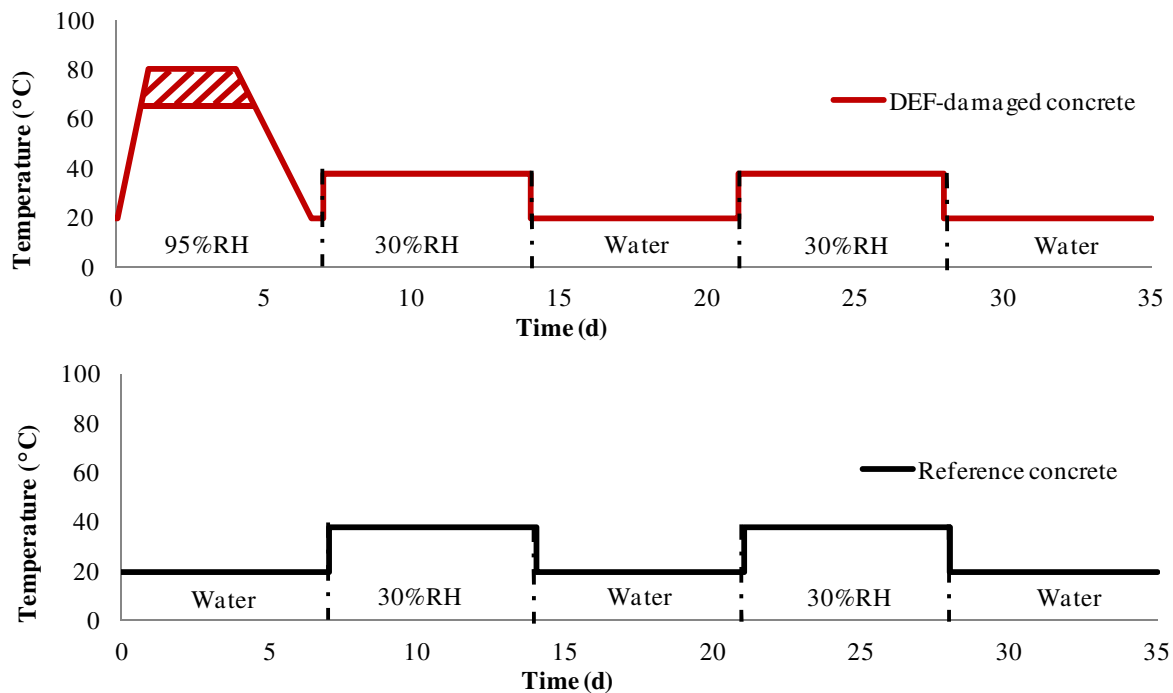
The mix designs have already been studied in other experimental works, which make it possible to complete the database on the behavior of these concretes [8, 11]. The first study have highlighted the risk of DEF in these concretes under variable moisture conditions; a decrease of mechanical properties and an increase of transfer properties under DEF degradation have also been shown [8]. Moreover, the impact of accelerating tests method has studied on theses concretes at scale structure, in terms of concrete expansion in [11]. However, some modifications were made in the nature of aggregates used. Indeed, the limestone aggregates used in [8, 11] contain a part of siliceous phase which is not qualified with respect to the risk of Alkali-Silica Reaction (ASR). To avoid a possibly ASR gel formation, the limestone aggregates used in this study is qualified as non-reactive for ASR degradation. The proportion of aggregates was determined with respect to Dreux method in order to reproduce the same aggregate skeleton. The formulations are detailed in Table 2. The CEMII-Si and CEMI-Ca concretes contained siliceous and limestone aggregates, respectively, to show the impact of the nature of aggregates on DEF. The choice of siliceous and limestone aggregates respectively with CEMII and CEMI has been conducted to reproduce mix design representative of nuclear structures. They have also been used for concrete blocks, as part of a new platform test developed by the Radioprotection and Nuclear Safety Institute (IRSN), to study the impact of DEF degradation at scale structure. The concrete casting procedure used in this study followed the protocol of French standards [12, 13].

(a) CEMII-Si		(b) CEMI-Ca	
Material	Content (kg/m ³)	Material	Content (kg/m ³)
CEMIII/A-LL 42.5 R	350	CEM I 52.5 N	400
0/0.315	264	0/4	718
0.315/1	151	4/11.2	289
1/4	254	11.2/22.5	813
4/8	145	Effective water	185
8/12	399	Na ₂ O _{eq}	5
12/20	616		
Effective water	188		
Plasticizer	0,35		
Na ₂ O _{eq}	3,5		

91 *Table 2: Mix designs of “CEMII-Si” (a) and “CEMI-Ca” (b) concrete*

92 **2.2. Degradation process**

93 In order to allow rapid development of DEF, IFSTTAR Test N° 66 was adopted, with some
 94 modifications [14]. This test comprises four stages: concrete mixing, heat treatment, dry/wet
 95 cycles, and final immersion of samples in water at 20°C. The thermal treatment at young age
 96 corresponded to that in Al Shamaa’s study [8].

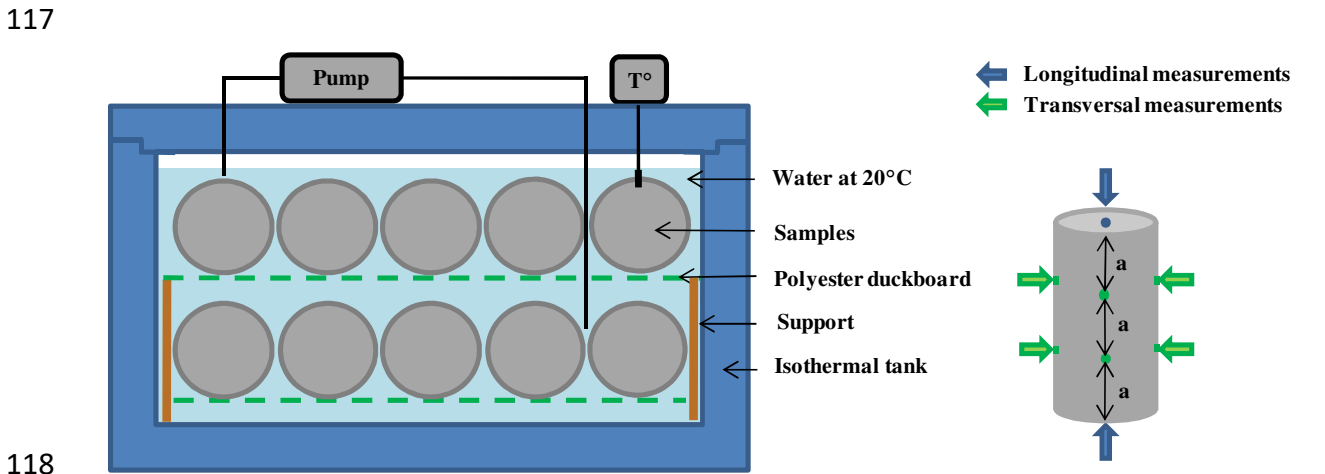


97
 98 *Figure 1: Thermal profile of concretes developing DEF and wet/dry cycles for both concretes*

99 Once cast, specimens were placed in a climate chamber at controlled temperature and relative
 100 humidity. The heat treatment was applied for 7 days and comprised four stages: a hold at
 101 20°C, 95% RH for 2h, followed by a rise in temperature from 20°C to 80°C, 95% RH at a rate

102 of 2.5°C/h. Stabilization at 80°C, 95% RH for 72h and a temperature decrease from 80°C to
103 20°C, 95% RH at a rate of 1°C/h (Figure 1).

104 As Kchachek and Brunetaud show, the maximum temperature reached in concrete is not the
105 only factor to be taken into account and it cannot be decoupled from the holding time [1,9].
106 The useful temperature generated by this duration of heat treatment is about 1240°C.h and
107 corresponds to the area under the curve of heat treatment for a temperature above 65°C in
108 Figure 1. The selected dry/wet cycles correspond to the accelerated protocol of IFSTTAR
109 Method N° 66 [15]. They are composed of two 14-day cycles: drying at 38°C, HR < 30% for
110 7 days and humidification in water at 20°C for 7 days (Figure 1). These cycles allow the
111 initiation of micro-cracking in the concrete and thus accelerate the kinetics of DEF
112 appearance within the concrete without increasing the amplitude of the deformations [2]. The
113 beginning of the degradation is considered to occur at 35 days, at the end of the heat treatment
114 and wet/dry cycles, in this case. During the first 35 days, the concrete is considered to be in a
115 state of hydration where no expansion due to DEF develops. The storage water is not
116 renewed.



119 Figure 2: Sample storage and measurements of dimensions

120 When the wet/dry cycles had been completed, the samples were stored in isothermal
121 containers at 20°C, equipped with a pump to homogenize the temperature and the species
122 present in the water (Figure 2). The reference specimens underwent the same elaboration
123 process but were not subjected to the heat treatment. During the first 7 days, the reference
124 specimens were stored in water at 20°C instead of being heated. Wet/dry cycles were also
125 applied (Figure 1).

126 The mass and expansion monitoring was performed on three cylindrical test pieces (11 x 22
 127 cm). The shrinkage plots were fixed directly on the mold and were therefore embedded in the
 128 concrete. Longitudinal expansion was measured by a digital micrometer having an accuracy
 129 of $\pm 1 \mu\text{m}$. The transversal expansion was measured by a micrometer having an accuracy of ± 5
 130 μm (Figure 2).

131 **2.3. Test protocols**

132 The physicochemical and mechanical tests performed during the experiments are listed in
 133 Table 3.

Chemical tests	Physical tests	Mechanical tests
pH of pore solution	Electrical resistivity	Compressive strength
Portlandite content	Chloride migration	Static moduli
SEM observation	Water porosity	Dynamic moduli
Alkali content	Gas permeability	

134 *Table 3: Physicochemical and mechanical tests performed during the experiments*

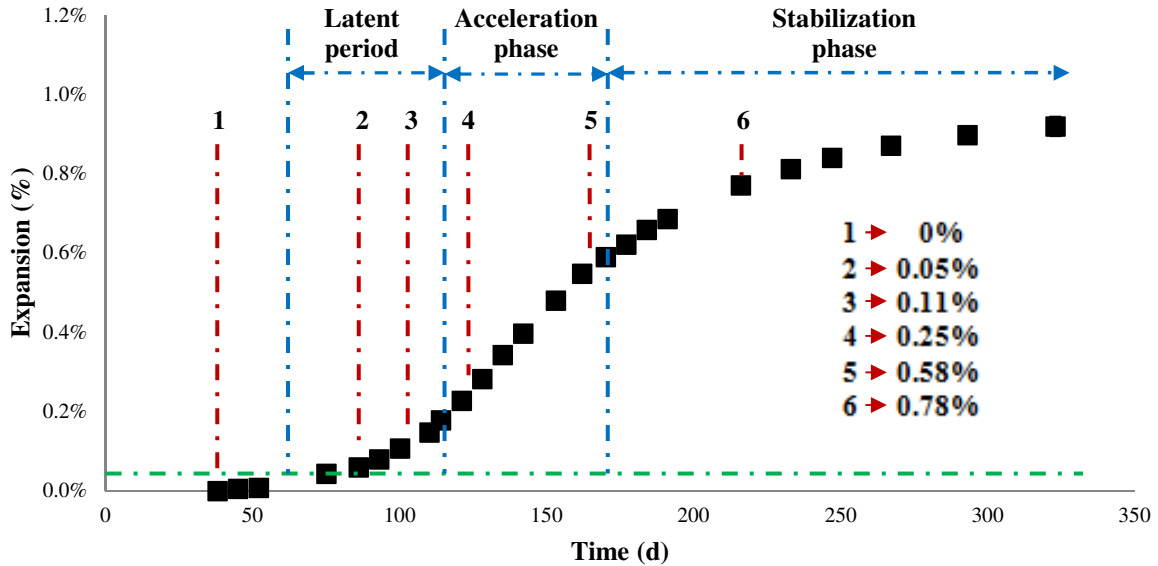
135 In order to observe the evolution of the physicochemical and mechanical properties of
 136 concrete during its degradation by DEF, chemical analyses were performed to ensure the
 137 presence of pathologies in the concrete. When the pathology was initiated (expansion of
 138 0.04%), measurement of the physical properties revealed the impact of the micro-cracking
 139 generated on the transfer properties. Finally, measuring the mechanical properties gave some
 140 indications on the state of damage of the concrete subjected to these pathologies.
 141 Measurements of all the properties were made at the different degrees of expansion shown in
 142 Figure 3. **The expansion curve due to DEF can usually be described as a sigmoid (Fig. 3),**
 143 **with three phases:**

144 - **The latent period is characterized by the precipitation of DEF in the microstructure**
 145 **(Porosity, Interface Transition Zone (ITZ), Hadley grain) [1]. Expansion is small in this**
 146 **period. When the tensile strength of concrete is reached due to internal pressure, cracks were**
 147 **generated.**

148 - **The precipitation of DEF in cracks, leads to cracks propagation and so to the acceleration of**
 149 **expansion.**

150 - **Finally, the deceleration of swelling occurs when one reactant is consumed and/or when the**
 151 **cracks opening is sufficiently significant to accommodate new products without generation of**
 152 **supplementary expansion [1].**

153 In order to detect the presence of DEF, the first characterization was conducted after curing in
 154 the initial state, at 35 days. When swelling begins, during the latent period, two
 155 characterizations were performed. Two other measurements were carried out during the
 156 acceleration phase and a final characterization was performed during the stabilization period.



157 *Figure 3: The 6 levels of expansion for the measurement of properties*
 158

159 **2.3.2. Chemical tests**

160 Two chemical tests were performed: pH measurement and determination of portlandite
 161 content.

162 The pH measurement was carried out on an 11 x 22 cm cylindrical specimen. The test piece
 163 was broken in compression. The pieces present in the center of the specimen were placed in a
 164 press to extract the interstitial solution present in the concrete. The pH was measured by a
 165 probe. The pore solution was then stabilized by acid and analyzed by Inductively Coupled
 166 Plasma Mass Spectrometry (ICP-MS) to determine the elements and their amounts.

167 The portlandite content was experimentally determined by Thermo-Gravimetric Analysis
 168 (TGA) on a sample taken from an 11 x 22 cm cylindrical specimen. The central part of the
 169 test piece was broken into small pieces and dried in a lyophilizer for 1 day. This part was then
 170 polished and metallized for Scanning Electron Microscopy (SEM) observation to check that
 171 DEF was present in the concrete.

172 **2.3.2. Physical tests**

173 Four physical tests were performed: electrical resistivity, chloride migration, porosity
 174 measurements, and gas permeability.

175 The electrical resistivity and non steady state chloride migration tests were performed
176 according to the standard, on the same three 11 x 5 cm cylindrical samples obtained from an
177 11 x 22 cm one [15,16]. The saturated concrete solution of the tests was replaced by a NaOH
178 concentration of 0.1 mol/l according to a new test protocol (PerfDub).

179 Gas permeability and water porosity tests were performed according to the standards [17, 18].
180 However, the drying temperature has been adopted at 40°C for two reasons: this helps to
181 avoid the destabilization of the delayed ettringite formed during the development of ISR and
182 on the other hand allows limiting the additional cracking caused by drying to 105°C, proposed
183 in the standards. In this case, the evolution of gas permeability during the expansion will
184 mainly due to concrete DEF damage by limiting supplementary cracks due to high drying
185 temperature.

186 2.3.1. Mechanical tests

187 Three mechanical properties were measured: the compressive strength, and the static and the
188 dynamic moduli. Linear and nonlinear acoustic methods were employed to determine the
189 dynamic moduli.

190 Compressive strength and static moduli were measured on three 11 x 22 cm cylindrical
191 specimens according to the standards [19, 20].

192 Several tests in development to determine the dynamic moduli are presented in the literature.
193 These tests have already been performed in the case of DEF damage [1, 8]. In this study, the
194 dynamic moduli was determined by two measurements. Linear acoustic emission was
195 performed in transmission and reception on the same specimens. The equipment used
196 included a SOFRANEL 5077PR signal generator, a TEKTRONIX oscilloscope and 250 kHz
197 longitudinal and transversal wave transducers. To improve the signal quality, a viscous liquid
198 was needed at the concrete/transducer interface; in this test, honey was used. The dynamic
199 moduli was determined from equation 1:

$$200 \quad E_{dyn} = \rho \cdot V_t^2 \cdot \left(\frac{3 \cdot V_l^2 - 4 \cdot V_t^2}{V_l^2 - V_t^2} \right) \quad (1)$$

201 with E_{dyn} the dynamic moduli (Pa), ρ the density in kg/m³, V_t the shear wave velocity (m/s),
202 V_l the compression wave velocity (m/s).

203 A nonlinear acoustic emission method was also used to evaluate the dynamic moduli. The
204 principle is to generate a pulse at the base of the test piece using a hammer. The resonance of
205 the specimen generates a signal collected by an accelerometer on the other side of the

206 specimen and treatment of the signal by a Fourier transformation gives the natural frequency
 207 of longitudinal resonance of the material. The moduli is then determined by equation 2:

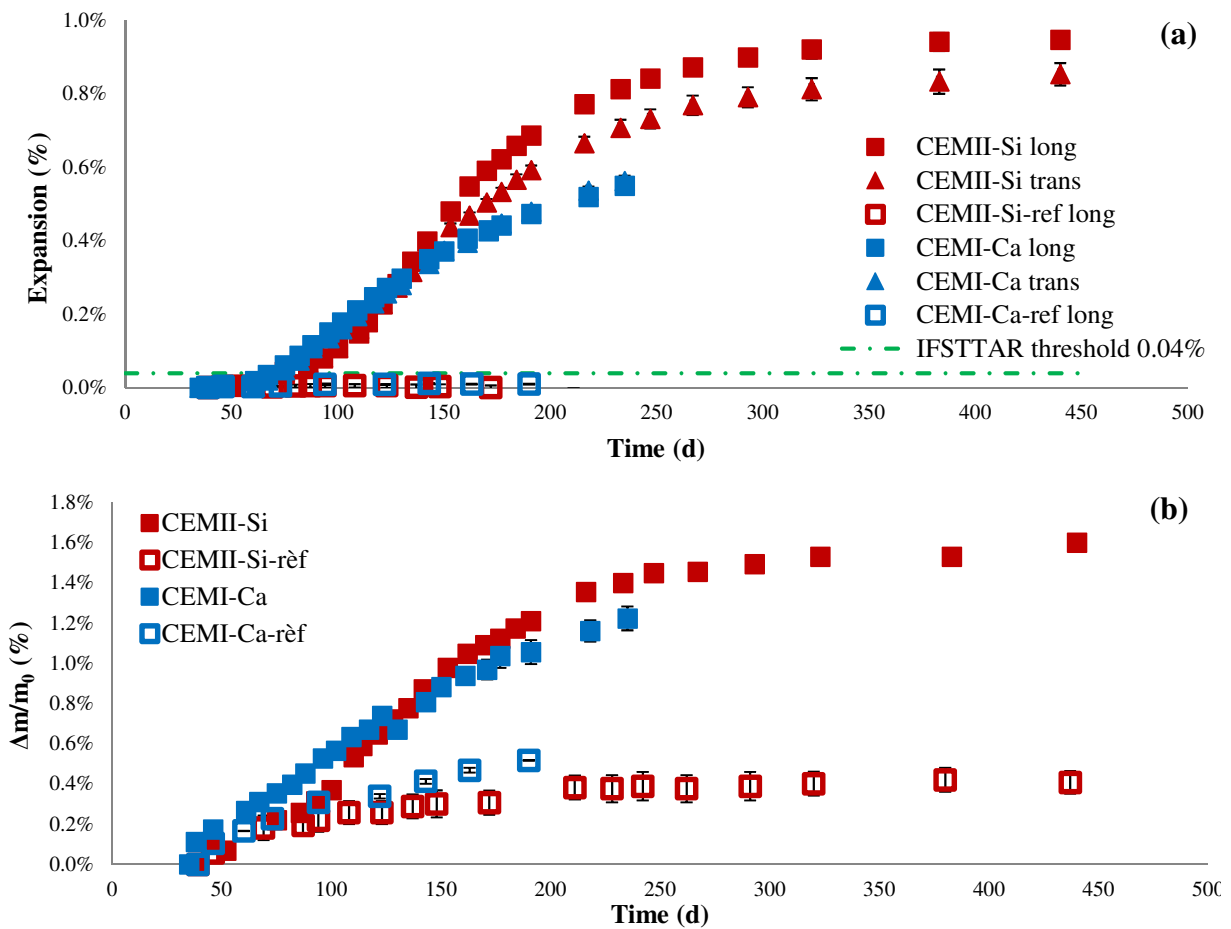
208
$$f_{long} = \frac{1}{2L} \sqrt{\frac{E_{dyn}}{\rho}} \quad (2)$$

209 with L the specimen length (m) and f_{long} the longitudinal natural frequency of the material
 210 (Hz).

211 **3. Experimental results**

212 **3.1. Expansion**

213 Figure 4a shows the evolution of expansion as a function of time for the CEMII-Si and
 214 CEMI-Ca concretes and their corresponding references CEMII-Si-ref and CEMI-Ca-ref.
 215 IFSTTAR method n° 66 refers to a swelling limit of 0.04% in an expansion test [14]. Beyond
 216 this threshold, there is a risk of the concrete being damaged by DEF. The reference
 217 formulations did not exceed the limit threshold and showed a maximum swelling of 0.02%.

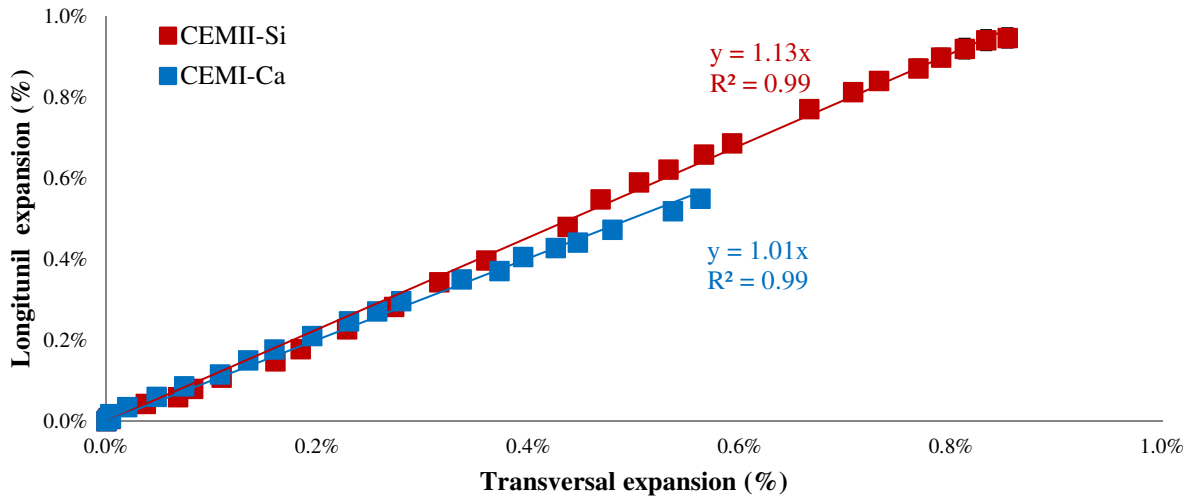


218 Figure 4: Evolution of expansion (transversal and longitudinal) (a) and mass gain (b) versus
 219 time

220 Specimens developing DEF showed significant swelling, around 0.9%, at the end of the
221 expansion for CEMII-Si. The latent period began at around 70 days, or 35 days after curing.
222 For the CEMI-Ca design, this period started at 60 days and ended quickly. The first point of
223 inflection was at 80 days for the CEMI-Ca and 110 days for the CEMII-Si concrete. CEMI-Ca
224 contained large limestone aggregates that lead to a decrease of the latent period [21]. This
225 phenomenon is attributed to the higher bonding in case of limestone aggregates with the
226 cement matrix. In this case, cracks generated at the ITZ during the heat treatment due to a
227 differential dilatation coefficient between paste and aggregates, were reduced [21]. On the one
228 hand, the low cracking results in a lower volume available to accommodate the new phases
229 due to DEF without inducing cracking and expansion. On the other hand, the low cracking
230 leads to a decrease of transfers properties in concrete and thus to delay DEF expansion. These
231 two phenomena are opposed. Indeed, a decrease in transfer properties cannot explain the
232 lowest latency period observed in the case of limestone aggregates. The decrease in available
233 volume caused by the low cracking at the ITZ therefore seems to be the cause of the decrease
234 in latency period. In this case, the volume of DEF necessary to generate pressure is reduced
235 and it leads to a decrease of latent period.

236 The final expansion of CEMI-Ca showed a swelling of around 0.6%. This lower swelling was
237 attributed to the presence of limestone aggregates, which allowed the bond between aggregate
238 and cement paste to be increased by the formation of calcium hydrates around the aggregates
239 and equally due to a high mechanical interlocking behavior [5, 22, 23, 24]. The cracks
240 generated by DEF at the ITZ were also reduced, allowing a lower final expansion [5, 23].

241 Figure 4b shows the evolution of mass as a function of time. The initial mass, m_0 , was
242 measured at 35 days. Reference samples have a mass gain of 0.4% stabilizing around 200
243 days. This increase was due to their storage in water at 20°C. For CEMII-Si and CEMI-Ca
244 concretes, the mass increase was proportional to the swelling of the concrete. In addition, the
245 kinetics of the mass gain for these two pathological concrete was in agreement with the
246 kinetics of swelling, which confirms the short latent period in the CEMI-Ca specimens
247 (Figure 4a). The mass gain of CEMII-Si and CEMI-Ca concrete reached respectively 1.5 and
248 1.2% at the end of expansion.



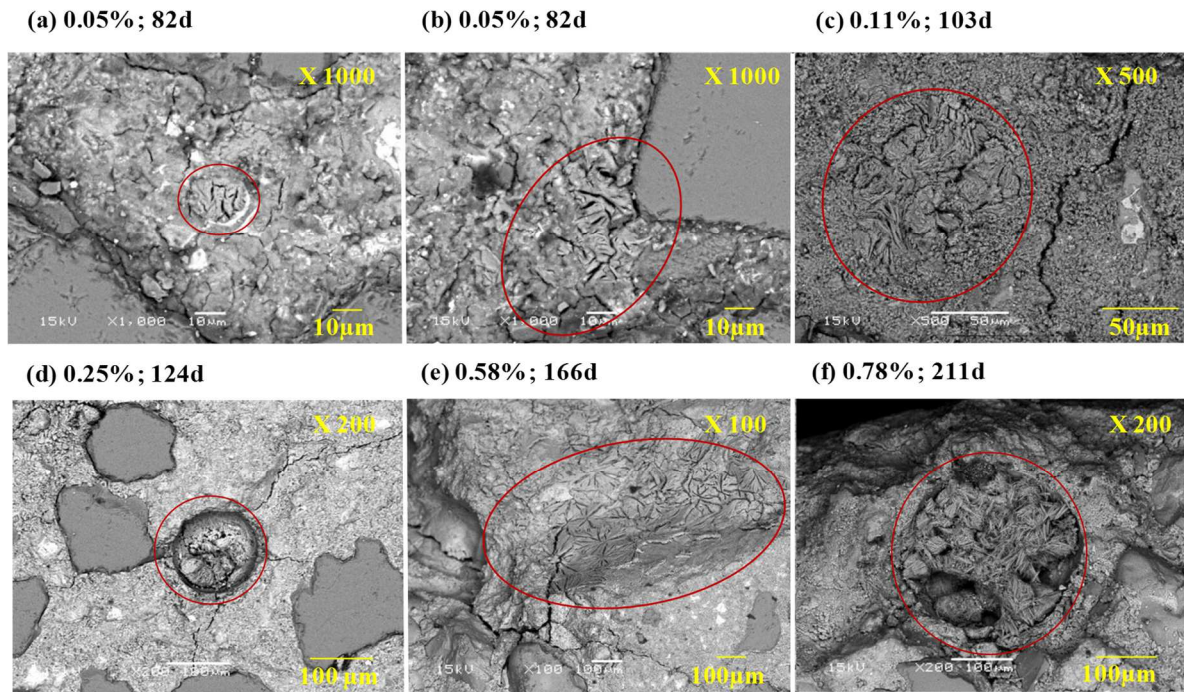
249
250

Figure 5: Evolution of longitudinal vs. transversal expansion

251 The longitudinal and transversal expansion measurements reported in Figure 5 are
252 proportional. The slope of proportionality is equal to 1, confirming the isotropy of the
253 swelling already observed in stress free conditions [25]. However, the transversal swelling is
254 slightly lower on the CEMII-Si concrete at the end of expansion.

255 *3.2. Microstructure evolution*

256 The presence of delayed ettringite was observed by SEM for each degree of expansion.

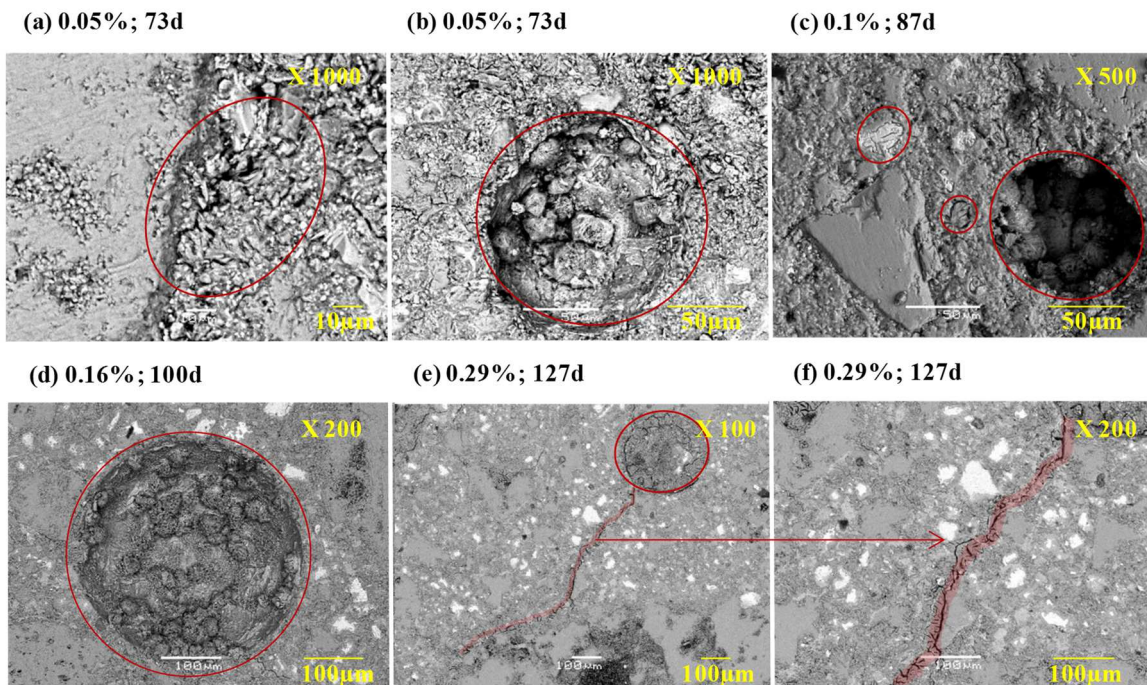


257

258

Figure 6: SEM images of the CEMII-Si concrete

259 Figure 6 shows the presence of delayed ettringite in massive and compressed form for
 260 different degrees of swelling. In the CEMII-Si formulation, siliceous aggregates were used.
 261 The SEM images show that the initiation of swelling was induced by the formation of delayed
 262 ettringite in Hadley grains (Figure 6a) and at the ITZ (Figure 6b). The swelling measured at
 263 this degree was 0.05%. As expansion continued, delayed ettringite continued to develop in
 264 these areas and in the porosity (Figure 6c and 6d). Then there was a separation from the
 265 cement paste all around the aggregates (Figure 6d). At the time corresponding to 0.25% of
 266 swelling, the cracks propagated from this interface to the porosity, causing an acceleration of
 267 swelling. When expansion continued, the presence of delayed ettringite became increasingly
 268 significant, both in the cement paste (Figure 6e) and in the porosity (Figure 6f).
 269

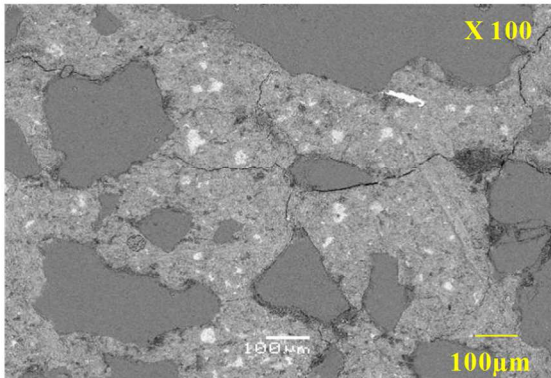


270
 271

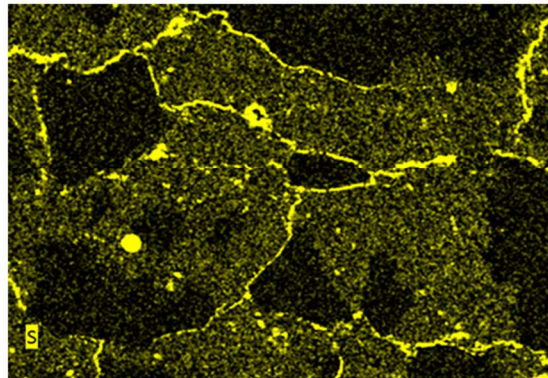
Figure 7: SEM images of the CEMI-Ca concrete

272 The SEM observations on the CEMI-Ca were consistent with those observed on the CEMII-Si
 273 concrete as ettringite developed primarily at the ITZ, in the Hadley grains and in the porosity
 274 (Figures 7a and 7b). As expansion continued, delayed ettringite continued to propagate in
 275 these areas (Figures 7c and 7d). When these preferential zones began to be completely filled
 276 by ettringite, the cracking propagated between them (Figures 7e and 7f) and the ettringite
 277 gradually began to fill the generated cracking. This step marked the acceleration of the
 278 degradation. However, cracking generated at the ITZ in the case of limestone aggregates did
 279 not propagate all around the aggregate, thus confirming the observations of Yang et al. [23].

(a) 0.92%; 320d



(b) 0.92%; 320d



280

281 Figure 8: CEMII-Si SEM images (a) initial image and (b) sulfur image (mapping)

282 These results show that, for each formulation, the presence of delayed ettringite is found first
283 at the ITZ in the Hadley grains and in the porosity. Ettringite then propagates in and between
284 these preferential zones, generating more and more cracking. This cracking marks the
285 acceleration of the expansion. As mentioned above, the cracking generated at the ITZ depends
286 on the nature of the aggregates [23]. In the case of siliceous aggregates, cracking is generated
287 all around the aggregate but it only partially surrounds limestone aggregates. Ettringite then
288 spreads in existing fissures. Figure 8b shows the presence of sulfur in the sample (yellow in
289 Figure 8b), proving the presence of delayed ettringite in concrete cracks. These observations
290 confirm that the cracks caused by the pathology are filled with ettringite during the expansion.
291 Recently, Brunetaud [1] had proposed a global swelling theory to explain the DEF
292 propagation. This theory is based on a homogeneous swelling of concrete. Delayed ettringite
293 would initially form in Hadley grains and porosity. The pressure generated by the DEF in the
294 cement matrix would lead to the presence of cracks at the ITZ (rigid inclusion) and the
295 development of delayed ettringite in this area. The crystallization pressure generated by the
296 formation of ettringite in these areas would lead to cracks propagation and thus accelerate the
297 degradation. These results are in agreement with this theory: delayed ettringite was first
298 observed in the Hadley grain, in the porosity and at the ITZ. Then delayed ettringite was
299 observed in the cracks.

300 3.3. Detection criterion

301 The first aim of this experimental work was to find a very sensitive test allowing DEF
302 detection. DEF can be detected if the evolution of one of the properties measured in this work
303 is significant (sufficiently higher than the scatter on results) and only due to DEF expansion
304 (not to concrete hydration). In this aim, a DEF detection criterion for physicommechanical

305 properties was developed, taking the effect of hydration and experimental scatter into account
 306 (equation 3).

$$307 \quad X_{i \text{ threshold}}(t) = X_0 \left(1 + \frac{X_{i \text{ ref}}(t) - X_{0 \text{ ref}}}{X_{0 \text{ ref}}} \right) \pm 2\overline{\sigma_{\text{ref}}} \quad (3)$$

308 with $X_{i \text{ threshold}}(t)$ the threshold value of detection of the property measured in time, X_0 the
 309 initial value of the pathological concrete, $X_{0 \text{ ref}}$ the initial value of the reference concrete, $X_{i \text{ ref}}(t)$
 310 the value of the property of the reference concrete in time and $\overline{\sigma_{\text{ref}}}$ the average of the
 311 standard deviations obtained on the reference specimens.

312 For the measurement of the chemical properties, the high dispersion of results did not allow
 313 this criterion to be used.

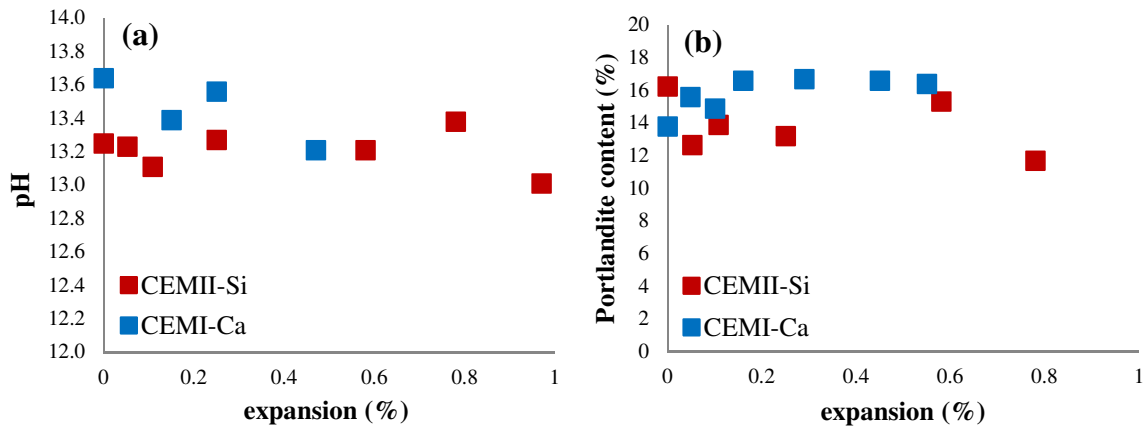
314 **3.4. Chemical properties**

315 ***3.4.1 pH measurement and portlandite content***

316 The pH analysis of the interstitial solution was performed for different degrees of expansion.
 317 Figure 9a shows the evolution of the pH for the CEMII-Si and CEMI-Ca concretes and Table
 318 4a summarizes the pH results obtained on the reference concretes. No significant change in
 319 the pH was observed on the reference specimens or on those developing the pathology (Table
 320 4a and Figure 9a). The pH of the interstitial solution of CEMII-Si concrete remained stable at
 321 a value of approximately 13.3 and that of the CEMI-Ca was also stable during the expansion,
 322 at around 13.4. The associated reference specimens showed the same trends, with pH around
 323 13.4 for CEMII-Si-ref and around 13.5 for CEMI-Ca-ref.

(a)	35d	90d	180d	(b)	(wt.%)	35d	90d	180d
CEMII-Si-ref	13.5	13.3	13.4	CEMII-Si-ref	13.4	11.9	11.4	
CEMI-Ca-ref	-	13.7	13.3	CEMI-Ca-ref	15.7	15.9	17.3	

324 Table 4: pH (a) and portlandite (b) evolution over time for reference concretes



325
326 *Figure 9: pH (a) and portlandite (b) evolution versus expansion for concretes damaged by*

327 DEF

328 The leaching of alkalis should have lowered the pH to about 12.6 over time, due to portlandite
329 pH buffering [26]. The test protocol may have been partly responsible for these stable, high
330 pH values. Chappex and Scrivener observed an increase in alkali concentrations in
331 accordance with the pressure applied up to 800 MPa [27]. During the present test, the pressure
332 was about 900 MPa. It is possible that the alkalis adsorbed physically on the surface of the
333 hydrates were released into the solution, leading to a pH buffering.

334 The evaluation of portlandite content performed by ATG on concrete samples (Figure 9b)
335 shows that it remained stable during the degradation, at between 11 and 17% for all concretes.
336 The oscillation of the values was a consequence of the sample used. This test is usually
337 performed on cement paste.

338 X-Ray Diffraction (XRD) analyses were conducted on the same samples. During the
339 degradation, no new formed phase was observed. The delayed ettringite being poorly
340 crystallized, its presence was not detected. In addition, the large peaks of calcite or silica,
341 depending on the nature of the aggregates used, masked the hydrated phases, thus making the
342 analysis complex.

343

344

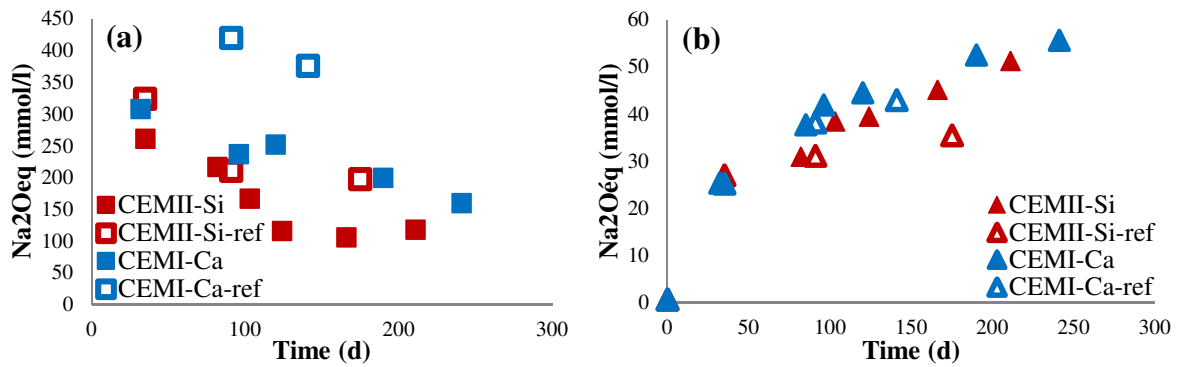
345

346

347

348

349 **3.4.2 Alkali concentrations**



350
351 Figure 10: Evolution of the equivalent alkali content in the interstitial solution (a) and in the
352 storage water (b) versus time

353 Figures 10a and 10b represent the evolution of the equivalent alkali content, expressed in
354 mmol/l, contained in the interstitial solution and in the storage water, respectively, for each
355 concrete. Figure 10b shows the strong leaching of alkali during the first 35 days. In fact, the
356 initial $\text{Na}_2\text{O}_{\text{eq}}$ concentration of the storage water was 0.6 mmol/l. At 35 days, this water
357 contained a concentration of 25 mmol/l. This significant leaching came, in particular, from the
358 fact that micro-cracking was generated during the wet/dry cycles. Underwater storage,
359 resulting in alkali leaching, continued over time. However, the leaching of specimens
360 developing the pathology seems to be greater than that of the reference concretes. At 200
361 days, the storage water of concretes developing DEF was found to have a concentration of 50
362 mmol/l, against about 40 mmol/l for reference concretes. This supplement of leaching can be
363 attributed to micro-cracking in the material, generated by the swelling of DEF.

364 Figure 10a confirms these results. The alkali leaching of interstitial water is greater for the
365 pathological concretes. In addition, the concentration of $\text{Na}_2\text{O}_{\text{eq}}$ of the reference concretes
366 seems to stabilize after 100 days. This stabilization could be attributed to the filling of the
367 pores at the periphery of the test piece with calcite. This phenomenon has also been observed
368 and discussed by Thibaut [28]. However, although the initial amount of alkali in the CEMI-Ca
369 and CEMI-Ca-ref concretes was higher, the leaching generated during the first 35 days
370 significantly decreased their concentration. The $\text{Na}_2\text{O}_{\text{eq}}$ concentration of the CEMI-Ca and
371 CEMII-Si concretes was found to be close respectively 308 and 261 mmol/l at 35 days despite
372 the difference of alkali content in the initial state.

373 The measurement of the portlandite content and the pH of the interstitial solution showed no
374 evolution during the degradation. The significant leaching of alkali over time was mainly due

375 to the storage. These chemical properties do not make it possible to detect DEF during the
 376 degradation.

377 **3.5. Physical properties**

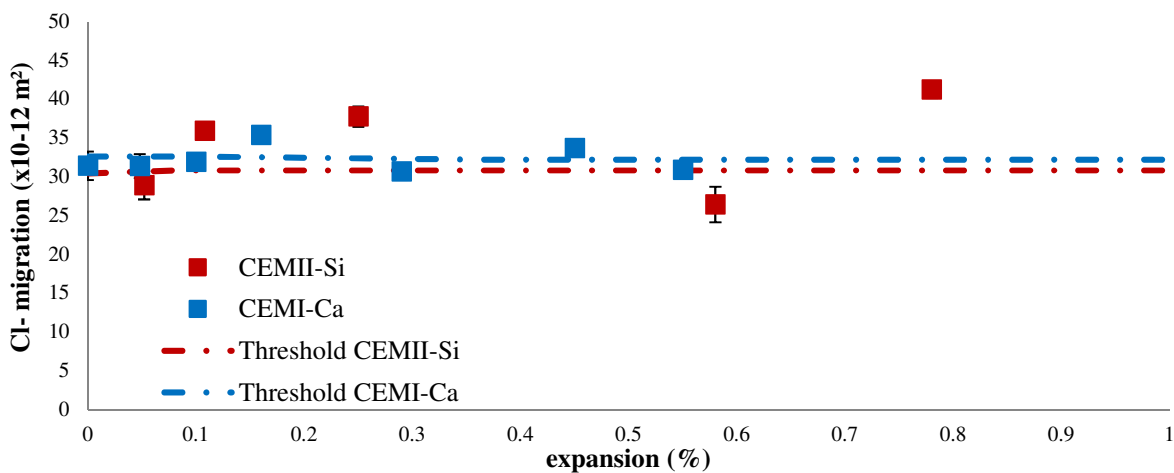
378 **3.5.1. Chloride migration**

379 Non steady state chloride migration tests and electrical resistivity measurements were
 380 performed on the same test specimens. Figure 11 shows the evolution of the chloride
 381 migration coefficient as a function of the expansion generated by the pathology. The CEMII-
 382 Si-ref and CEMI-Ca-ref references had a migration coefficient that hardly varied over time
 383 (by 13×10^{-12} and $11 \times 10^{-12} \text{ m}^2$ respectively (Table 5)).

($\times 10^{-12} \text{ m}^2$)	35d	90d	180d
CEMII-Si-ref	12.6 ± 0.2	12.8 ± 0.3	14.9 ± 1.8
CEMI-Ca-ref	10.3 ± 0.4	11.2 ± 0.3	10.2 ± 1.1

384 *Table 5: Evolution of the coefficient of migration of chlorine ions according to time for*
 385 *reference concretes*

386 Concretes developing pathology had a higher migration coefficient, around $30 \times 10^{-12} \text{ m}^2$,
 387 before DEF expansion. There are several reasons to believe that this increase in comparison
 388 with the reference concrete was due to the heat treatment effect. The heat treatment may have
 389 generated a modification of the composition of the cement paste and the hydrates formed
 390 [29]. In addition, the thermal expansion effects may have damaged the cement paste and the
 391 ITZ [21, 30].



392 *Figure 11: Evolution of the coefficient of migration of chlorine ions according to the*
 393 *expansion for concretes damaged by DEF*

395 For the concretes developing the pathology, no significant increase in the migration
 396 coefficient was observed. This phenomenon can be explained by the fact that the chloride ions
 397 diffused uniformly in the cement paste through the porosity and micro-cracking due to DEF
 398 after expansion. When measurements were taken, this generated a linear penetration front
 399 despite the presence of macro-cracking. The wide scatter of the results did not allow the
 400 detection of DEF.

401 3.5.2. Electrical resistivity

402 The electric resistivity tests (Figure 12) showed greater sensitivity. Reference concretes
 403 CEMII-Si-ref and CEMI-Ca-ref had a resistivity of 45 Ω .m at 35 days (Table 6). The
 404 concretes developing the pathology had a lower resistivity, around 35 Ω .m, at the same time,
 405 the heat treatment having caused additional damage.

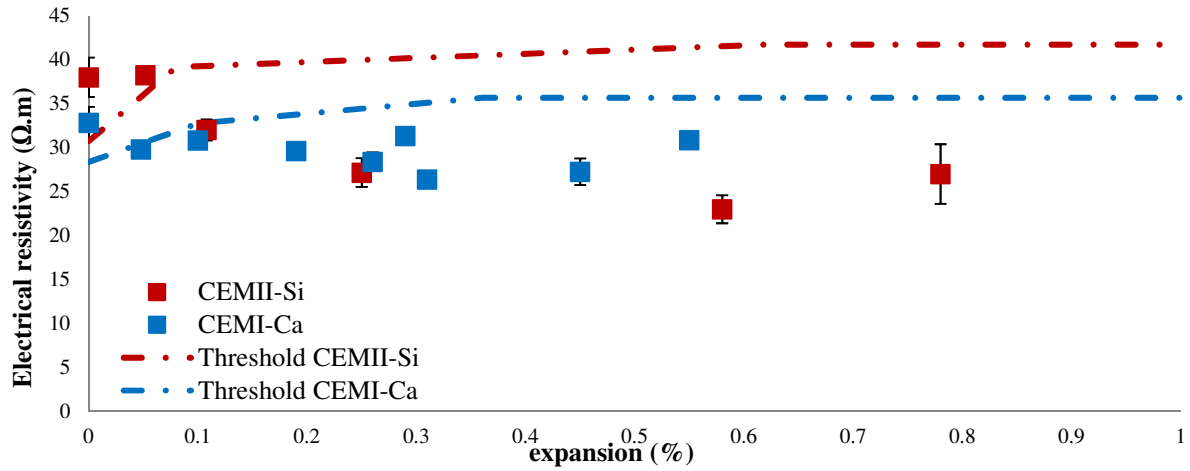
(Ω .m)	35d	90d	180d
CEMII-Si-ref	45.0 \pm2.2	55.0 \pm3.8	58.0 \pm4.9
CEMI-Ca-ref	45.0 \pm1.0	51.0 \pm1.7	55.0 \pm4.0

406 Table 6: Evolution of the electrical resistivity over time for reference concretes

407 In Figure 12, a gradual decrease in the resistivity is observed during the degradation for each
 408 pathological concrete. A threshold of around 25 Ω .m is reached at 0.3% expansion. This
 409 threshold of resistivity could be due to the cracking caused by the pathology being gradually
 410 filled by ettringite. In contrast, for the reference concretes, the electrical resistivity increased
 411 significantly between 35 and 90 days. A resistivity gain of 25% was observed from day 35 to
 412 day 180, due to the continuation of the hydration reactions causing a densification of the
 413 concrete.

414

415



416

417 Figure 12: Evolution of the coefficient of the electrical resistivity according to the expansion
 418 for concretes damaged by DEF

419 With the chosen criterion (Eq. 3), the detection of DEF took place between 0.05 and 0.1% of
 420 expansion, during the latent period. Between these two expansion levels, the decrease of
 421 resistivity was sufficient to point out significant damage.

422 3.5.3. Water porosity

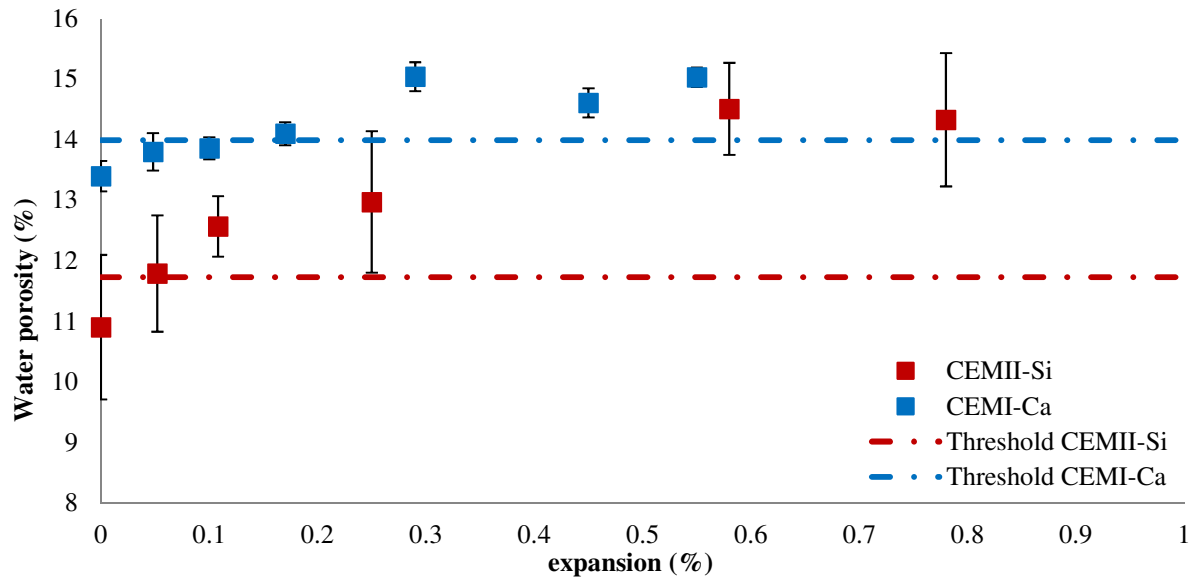
423 Figure 13 shows the evolution of the water-accessible porosity as a function of the expansion
 424 caused by DEF. The reference concretes CEMII-Si-ref and CEMI-Ca-ref show no evolution
 425 over time despite the continuation of hydration reactions (Table 7).

(%)	35d	90d	180d
CEMII-Si-ref	11.2 ±0.7	11.4 ±0.2	11.9 ±0.3
CEMI-Ca-ref	12.8 ±0.3	13.4 ±0.4	13.7 ±0.3

426

Table 7: Evolution of water porosity over time for reference concretes

427 The porosity measured on the CEMII-Si concrete remains lower than that measured on the
 428 CEMI-Ca concrete. The use of limestone aggregates of higher porosity for CEMI-Ca
 429 concretes could explain this difference, the water absorption coefficient of these aggregates
 430 being greater: 2.6% against 0.6%. When the concrete is damaged by delayed ettringite
 431 formation, porosity tends to increase, this being attributed to the formation of a crack
 432 network, filled by water. The increase in porosity is rapid at the beginning of the expansion
 433 and then stabilizes at the end of the expansion period. This stabilization can be explained by a
 434 competition between crack opening and crack filling with delayed ettringite.



435

436 *Figure 13: Evolution of water porosity as a function of expansion for concretes damaged by*

437

DEF

438 Depending on the criterion chosen, the detection takes place between 0.15 and 0.25% of
 439 expansion, at the beginning of the acceleration phase.

440 3.5.4. Gas permeability

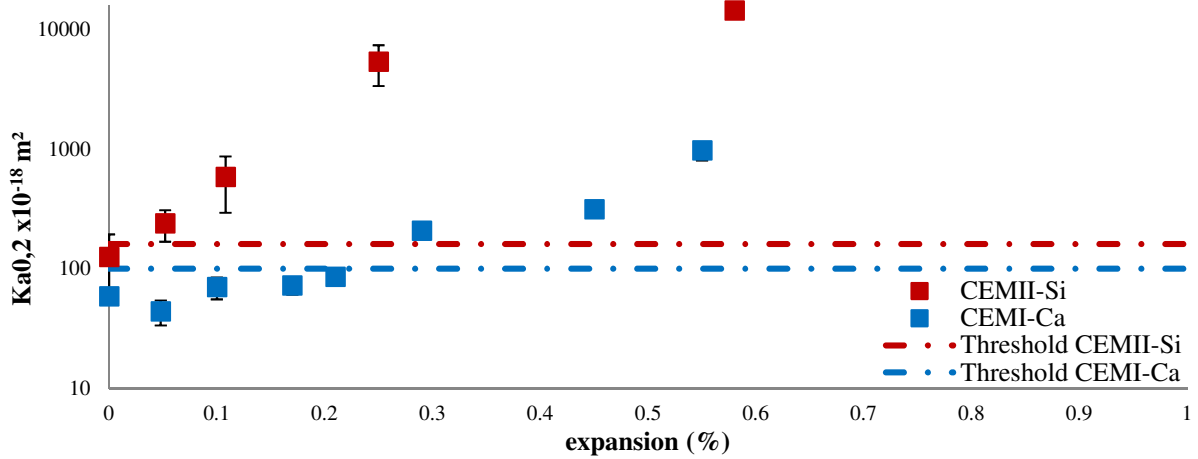
441 Figure 14 shows the evolution of the apparent air permeability coefficient according to the
 442 expansion generated by DEF. The reference concretes CEMII-Si-ref and CEMI-Ca-ref show
 443 no change in their coefficients of permeability over time of $110 \times 10^{-18} \text{ m}^2$ (Table 8).

($\times 10^{-18} \text{ m}^2$)	35d	90d	180d
CEMII-Si-ref	110 ±23	106 ±12	101 ±27
CEMI-Ca-ref	101 ±38	111 ±13	120 ±10

444 *Table 8: Evolution of apparent gas permeability coefficient over time for reference concretes*

445 The CEMII-Si and CEMI-Ca concretes developing the pathology have apparent gas
 446 permeability coefficients that are similar, respectively equal to $125 \times 10^{-18} \text{ m}^2$ and $60 \times 10^{-18} \text{ m}^2$
 447 before expansion. During expansion, the CEMII-Si concrete shows a strong increase in the
 448 coefficient of permeability at the beginning of expansion (permeability at 0.05% is double
 449 that before expansion). The CEMI-Ca also shows an increase but it occurs later and is
 450 smaller. This difference could be due to the mineralogical nature of the aggregates used. The
 451 ITZ of concretes containing limestone aggregates seems to be improved [5, 22, 23]. As
 452 mentioned above, cracks due to DEF passing through this interface are reduced in the case of
 453 limestone aggregates [23]. There may be fewer preferential paths in the CEMI-Ca concrete,

454 causing a smaller increase in the coefficient of permeability at early expansion. When the
 455 acceleration phase of the pathology is reached, at around 0.2% of swelling, the permeability is
 456 significantly impacted. This drastic increase can be attributed to the formation of more and
 457 more percolating paths within the material, generating a large increase of gas flow during the
 458 test. These results are therefore in agreement with those of Al Shamaa et al. [31].



459
 460 *Figure 14: Evolution of apparent gas permeability coefficient according to the expansion for*
 461 *concretes damaged by DEF*

462 Depending on the criterion chosen, the detection takes place during the latent period before
 463 0.05% expansion for CEMII-Si concrete and at the beginning of the acceleration phase,
 464 between 0.17 and 0.29%, for CEMI-Ca concrete.

465 3.6. Mechanical properties

466 3.6.1 Compressive strength

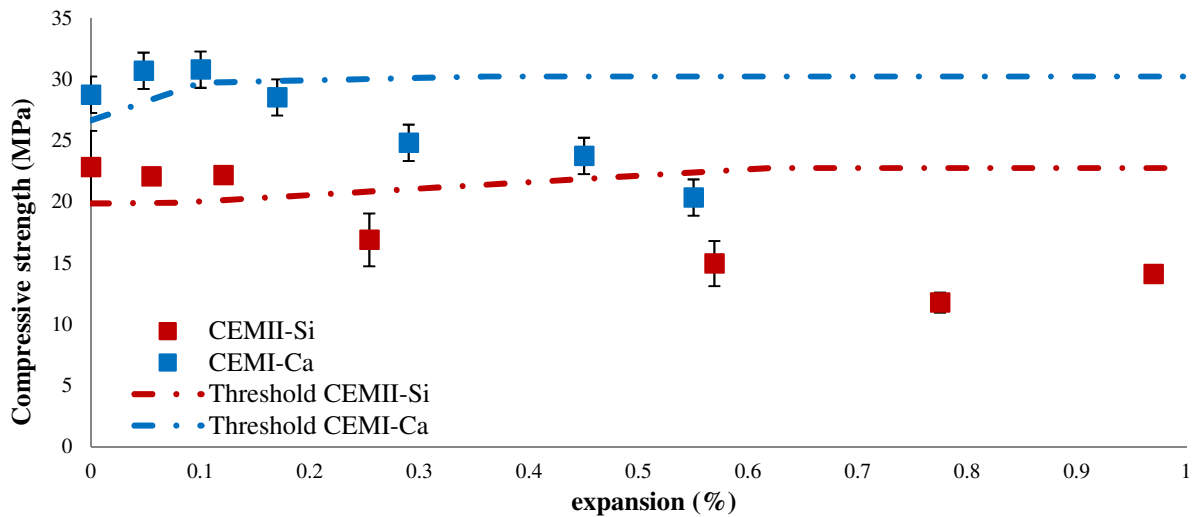
467 The compressive strength measurements also show the impact of the heat treatment on the
 468 mechanical properties. The reference concretes CEMII-Si-ref and CEMI-Ca-ref have
 469 compressive strengths of 34 MPa and 44 MPa, respectively, at 35 days (Table 9).

(MPa)	35d	90d	180d
CEMII-Si-ref	34.0 ±2.0	34.1 ±1.3	38.3 ±0.5
CEMI-Ca-ref	43.5 ±1.5	48.2 ±1,4	49.0 ±0.3

470 *Table 9: Evolution of the compressive strength over time for reference concretes*

471 The compressive strengths of CEMII-Si and CEMI-Ca are lower, at 23 MPa and 29 MPa,
 472 respectively. The reduction of the compressive strength by the heat treatment can be
 473 explained as previously by the occurrence of damage in the cement paste and the ITZ and by

474 the modification of the composition of hydrates [21, 29, 30]. The compressive strength of
 475 CEMI-Ca and CEMI-Ca-ref concretes remains higher than those of other concretes and
 476 increases with time following the hydration process. This difference is explained by the fact
 477 that these concretes contain a larger amount of cement and a lower W/C ratio, and also
 478 because the presence of limestone aggregates in the formulation improves the ITZ. The
 479 CEMII-Si and CEMI-Ca pathological concretes show compressive strength that remains
 480 stable during the initiation of the pathology. However, during the acceleration phase, the
 481 strength decreases spontaneously and then stabilizes at the end of the acceleration period.
 482 These results are in accordance with those of Bouzabata et al. [25]. The compressive strength
 483 drop is 30% and 20% for the CEMII-Si and CEMI-Ca concretes, respectively, at the middle
 484 of expansion.



485
 486 *Figure 15: Evolution of the compressive strength according to the expansion for concretes*
 487 *damaged by DEF*

488 Depending on the criterion chosen, the detection takes place between 0.17 and 0.25% of
 489 expansion, at the beginning of the acceleration phase.

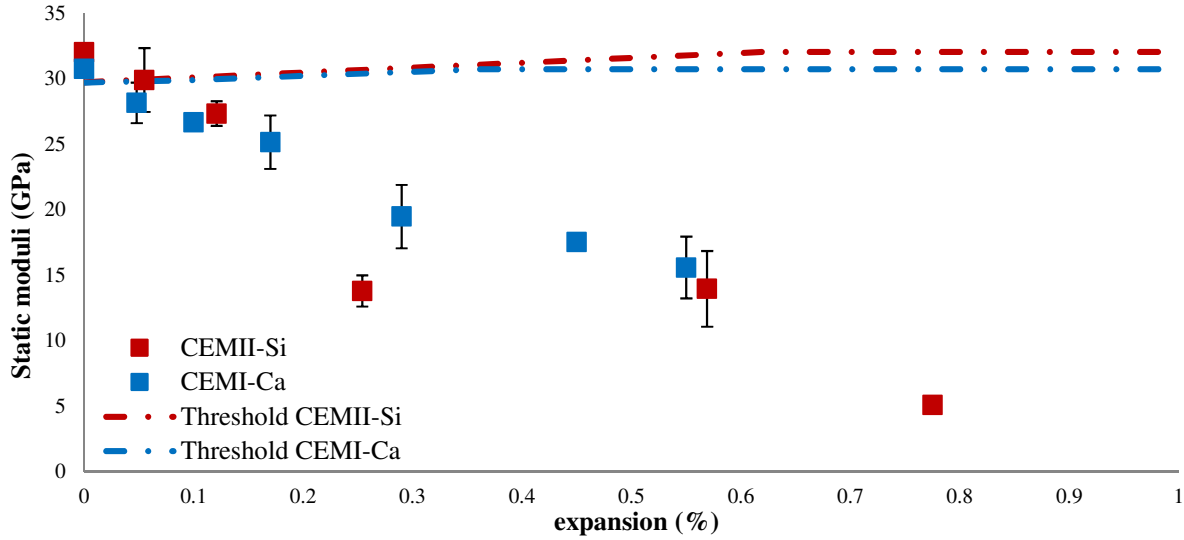
490 3.6.2 Static moduli

491 The static moduli of CEMII-Si-ref and CEMI-Ca-ref reference concretes shows small changes
 492 between 35 and 190 days (Table 10). The moduli is still higher for CEMII-Si-ref concrete
 493 (equal to 40 GPa) than for CEMI-Ca-ref concrete (31 GPa) at 35 days.

(GPa)	35d	90d	180d
CEMII-Si-ref	40.4 ±2.5	39.4 ±0.4	43.3 ±1.0
CEMI-Ca-ref	31.9 ±0.01	32.1 ±0.5	33.0 ±0.5

494 *Table 10: Evolution of the static moduli as a function of time for reference concretes*

495 However, the CEMII-Si and CEMI-Ca pathological concretes reveal that the moduli
 496 decreases progressively during the expansion. A significant decrease in the moduli is
 497 observed for swelling of around 0.2% during the acceleration phase of the pathology (Figure
 498 16). At this time, the moduli decreases by 40% and 50% for the CEMII-Ca and CEMII-Ca-ref
 499 concretes, respectively. The loss of static moduli seems to be proportional to the expansion
 500 rate caused by the pathology. These results are not in agreement with those of Al Shamaa et
 501 al., who show no decrease of static moduli during the latent period [10].



502
 503 *Figure 16: Evolution of the static moduli according to the expansion for concretes damaged*
 504 *by DEF*

505 Depending on the criterion chosen, the detection takes place between 0.05 and 0.1% of
 506 expansion, during the latent period.

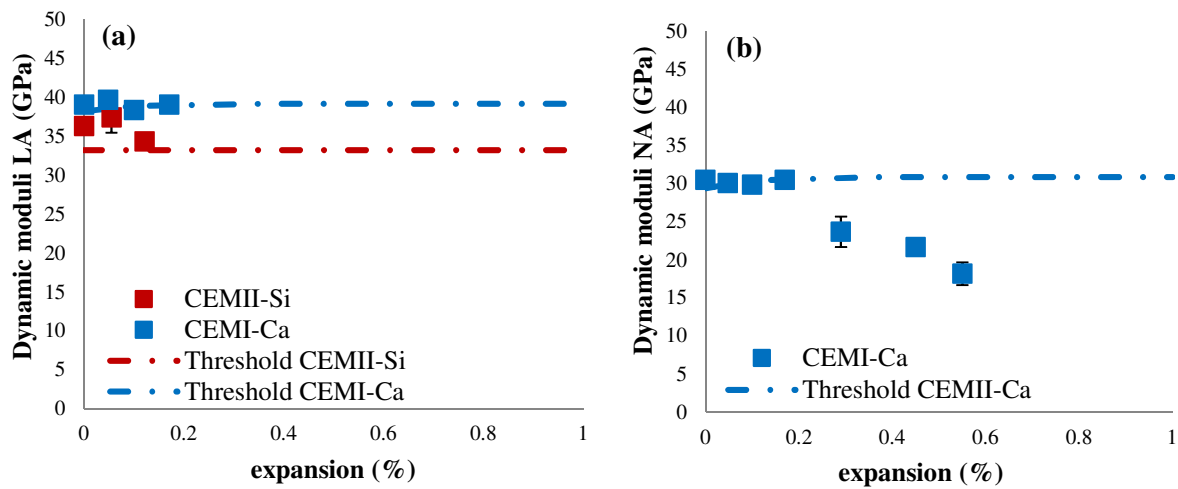
507 **3.6.3 Dynamic moduli**

508 Figure 17a shows the evolution of the dynamic linear acoustic moduli according to expansion.
 509 The reference concretes CEMII-Si-ref and CEMI-Ca-ref show no moduli evolution over time
 510 (moduli of about 45GPa and 41GPa, respectively, by linear acoustics Table 11a).

	(GPa)	35d	90d	180d
(a)	CEMII-Si-ref	44.5 ±1.5	48.4 ±0.8	43.3 ±0.9
	CEMI-Ca-ref	40.9 ±0.6	41.6 ±0.5	41.9 ±0.2
(b)	CEMII-Si-ref	-	-	-
	CEMI-Ca-ref	33.5 ±0.5	34.6 ±0.4	35.1 ±0.7

511 *Table 11: Evolution of the dynamic moduli in linear (a) and nonlinear (b) acoustics over time*
 512 *for reference concretes*

513 The CEMII-Si and CEMII-Ca pathological concretes have dynamic moduli of 36 GPa and 39
 514 GPa, respectively, and only the dynamic moduli of the CEMII-Si concrete seems to be
 515 impacted by the heat treatment. This difference can be explained by the difference of ITZ
 516 between these aggregates [21, 30]. For the pathological concretes, no evolution of the
 517 dynamic moduli measured by linear acoustics is observed during the expansion. When the
 518 damage becomes too great, during the acceleration phase, the received signal becomes too
 519 disturbed. It follows that a very weak signal is detected by the sensor in reception, making the
 520 measurements unusable (linear acoustics).



521
 522 Figure 17: Evolution of the dynamic moduli in linear (a) and nonlinear (b) acoustics
 523 according to the expansion for concretes damaged by DEF

524 Dynamic moduli measurements in nonlinear acoustics (Figure 17b) show the same trend. The
 525 dynamic moduli remains stable around 35 GPa over time for the reference concrete (Table
 526 11b). The dynamic moduli of the pathological concrete CEMI-Ca remains slightly lower than
 527 that of the reference concrete, 30 GPa at 35 days. However, it decreases rapidly around 0.2%
 528 of expansion during the acceleration phase of the pathology. The loss of moduli associated
 529 with the development of the DEF is of the order of 30% at 0.45% of expansion. These results
 530 are in agreement with those found in the literature [10, 31, 32, 33].

531 Depending on the criterion chosen, detection by nonlinear dynamic moduli takes place
 532 between 0.17 and 0.29% of expansion, at the beginning of the acceleration phase. The linear
 533 dynamic moduli does not allow DEF to be detected.

534
 535
 536

537 **4. Discussion**

538 **4.1. Detection of DEF**

539 The results obtained on the evolution of the concrete properties according to expansion show
 540 that only some particular tests make it possible to detect DEF at the beginning of the
 541 expansion, during the latent phase. Table 12 summarizes all the expansion values at the time
 542 of detection of pathologies presented in the experimental results.

	Expansion at detection (%)		DEF phase
	CEMII-Si	CEMI-Ca	
pH of pore solution	-	-	-
Portlandite content	-	-	-
Chloride migration	-	-	-
Electrical resistivity	0.05-0.11	0.05-0.11	Latent phase
Water porosity	0.11-0.25	0.17-0.29	Acceleration phase
Gas permeability	0.05	0.17-0.29	Latent phase
Dynamic moduli AL	-	-	-
Dynamic moduli NA	-	0.17-0.29	Acceleration phase
Static moduli	0.05 / 0.11	0.05-0.11	Latent phase
Compressive strength	0.11 / 0.25	0.17-0.29	Acceleration phase

543 *Table 12: Summary of the evolution of the properties at detection for the CEMII-Si and*
 544 *CEMI-Ca concretes*

545 Microscopic observations showed the evolution of ettringite formation during expansion in
 546 the material. However, measurements of pH and portlandite content showed no evolution
 547 during the expansion. The potential modification of portlandite when the pathology develops
 548 in the concrete cannot be identified by the technique used in this study. Some physical
 549 measurements related to the transfer properties allowed DEF to be detected during the latent
 550 phase and measurements of the gas permeability and electrical resistivity appear to provide a
 551 good sustainability indicator for the detection of DEF. The doubling of the apparent gas
 552 permeability coefficient at 0.12% of expansion for the CEMII-Si concrete reveals that the loss
 553 of containment occurs at a low degree of expansion for unreinforced concrete. However, the
 554 CEMI-Ca concrete showed a later increase in permeability coefficient, during the acceleration
 555 phase. The improvement of ITZ in the case of limestone aggregates seems to reduce the
 556 cracks generated at this interface during DEF damage [23]. Thus allowing the cracks in the
 557 concrete to be less percolating.

558 The electrical resistivity tests also showed significant sensitivity, the detection being effective
 559 from the latent phase. The electrical resistivity decreased by 16% and 10% for the CEMII-Si
 560 and CEMI-Ca concretes, respectively, for expansions of 0.12% and 0.19%. Since the

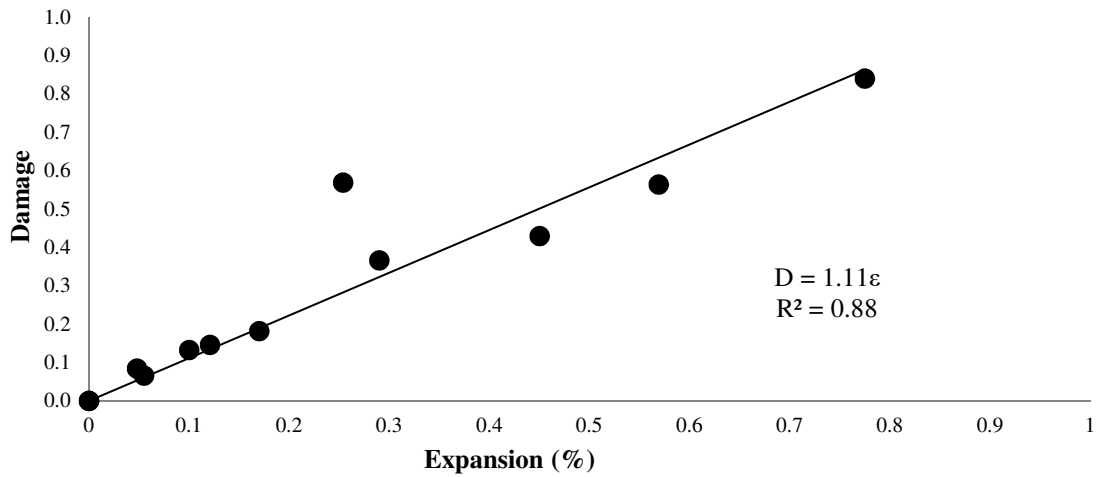
561 electrical resistivity of the reference concretes increased substantially from 35 days to 180
562 days, the decrease in the resistivity associated with the development of the pathology seems to
563 be significant. However, this parameter was very sensitive to the degree of saturation of
564 concrete [34]. In case of existing structure, electrical resistivity is commonly used to assess
565 the degree of saturation of concrete. So in case of DEF damage structure, it could be difficult
566 to use the electrical resistivity to determine both the degree of saturation and the occurrence
567 of DEF.

568 The water porosity measurements did not show any great sensitivity. The increase in porosity
569 associated with micro-cracks in the matrix was small compared to the initial pore volume,
570 making detection difficult. A relative increase of the porosity of 19% compared to the initial
571 porosity for a swelling of 0.25% was observed on the CEMII-Si concrete. At this degree of
572 expansion, cracking was already visible on the faces of the concrete specimens. Dynamic
573 moduli measurements in linear acoustics did not detect the presence of DEF in concrete but
574 tests in nonlinear acoustics showed a decrease in dynamic moduli when it was no longer
575 measurable by the previous method. A decrease of 22% for an expansion of 0.29% was
576 observed for the CEMI-Ca concrete at the middle phase of acceleration. Static moduli
577 measurements had greater sensitivity than the two previous methods and allowed detection
578 during the latent phase. A continuous decrease was observed throughout the development of
579 the pathology. A 15% loss of moduli associated with a swelling of 0.11% was observed for
580 each concrete. The compressive strength of the CEMII-Si and CEMI-Ca concretes damaged
581 by DEF decreased by 26% and 14% respectively for expansions of 0.25% and 0.29%. This
582 loss of compressive strength in the middle phase of acceleration delayed the detection of the
583 pathology. Three sustainability indicators made it possible to detect DEF earlier, during the
584 latent phase for laboratory specimens. These were the gas permeability, the electrical
585 resistivity and the static moduli.

586 **4.2. Sustainability of concretes damaged by DEF**

587 Figure 18 shows the evolution of the damage as a function of the expansion for the two
588 concretes undergoing DEF. In this study, the damage was proportional to the expansion due to
589 DEF. The damage was calculated from the static moduli according to Equation 4:

590
$$D = 1 - \frac{E_i}{E_0} \quad (4)$$



591

592

Figure 18: Evolution of the damage as a function of expansion

593

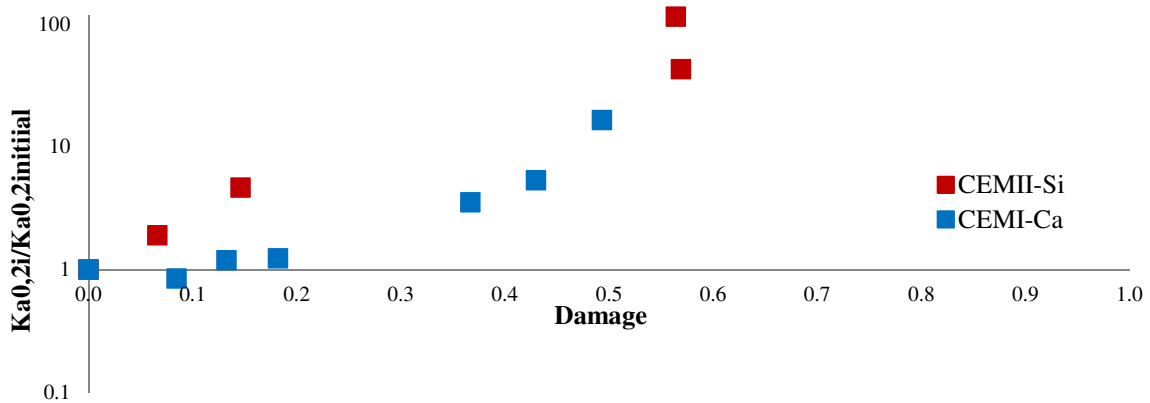
A study by Martin et al. on coupled AAR and DEF expansion on concrete shows an almost

594

linear trend. The loss of damage according to the expansion is in accordance with these results

595

[35].



596

597

Figure 19: Evolution of the apparent permeability rate as a function of damage

598

The evolution of the apparent gas permeability rate presented in Figure 19 shows that the

599

increase in the permeability seems to be an exponential function of the damage. However, the

600

percolating paths in CEMI-Ca concrete specimens would appear at around 20% of damage, at

601

the beginning of the acceleration phase of the pathology. For the CEMI-Si concrete, the

602

percolating paths appear for slight damage, around 7%, causing a considerable increase of the

603

air flow through the material. The greater bonding at the ITZ in the case of limestone

604

aggregates seems to allow the containment properties to be maintained during the beginning

605

of the DEF damage, when it is lower than 20%.

606

607

Potential Sustainability					
Sustainability indicators	Concretes	Initial state	Latent phase	Acceleration phase	Stabilization phase
Expansion (%)	CEMII-Si	0	0.02-0.15	0.15-0.7	0.8
	CEMI-Ca	0	0.02-0.1	0.1-0.45	0.55
Electrical resistivity	CEMII-Si	Very low	Very low	Very low	Very low
	CEMI-Ca	Very low	Very low	Very low	Very low
Gas permeability (40°C)	CEMII-Si	Medium	Low	Very low	Very low
	CEMI-Ca	High	High	Medium	Low
Water porosity (40°C)	CEMII-Si	High	Medium	Low	Low
	CEMI-Ca	Medium	Medium	Low	Low

608 *Table 13: Classification of concrete damaged by DEF relative to limit values for the potential*
609 *sustainability and properties of concrete [36]*

610 Table 13 shows the evolution of the potential durability of concretes during the development
611 of the pathology. The “low” classification at the initial state of concretes is mainly due to the
612 effects of heat treatment and wet/dry cycles as mentioned previously [21, 29, 30].
613 Sustainability indicators show lower potential sustainability as early as the latent period for
614 CEMII-Si concrete and this trend continues throughout the degradation. The presence of
615 limestone aggregates in CEMI-Ca concrete seems to maintain the same sustainability during
616 this phase. During the acceleration phase of the pathology, the potential sustainability of
617 concretes becomes greatly affected. This could accelerate the kinetics of appearance of other
618 pathologies such as AAR, carbonation and corrosion, causing premature aging of the
619 structures.

620 **5. Conclusion**

621 A large experimental program has been proposed in order to obtain a sensitive measurement
622 of DEF, allowing its detection before it can be observed visually. The second objective was to
623 evaluate the evolution of the properties that have an impact on the containment and on the
624 sustainability of concrete where other pathologies are also present. Numerous
625 physicochemical and mechanical properties were measured by the use of a large quantity of
626 samples. These tests were performed on two concretes showing a high swelling potential
627 when DEF occurs and containing aggregates of different mineralogical natures. First, it
628 confirms the results of the scarce studies reported in the literature:

- 629 • DEF expansion is isotropic in stress-free conditions [25].

630 • Microscopic observations have shown DEF development in accordance with the
631 theory of swelling proposed by Brunetaud [1].

632 Second, original results have been obtained on the durability indicators for concrete damaged
633 by DEF:

634 • The measurements of pH and portlandite content do not show any evolution during the
635 pathology in spite of strong leaching of alkalis.

636 • The measurement of physical properties shows that electrical resistivity and gas
637 permeability are sensitive to the expansion generated by DEF, the detection being
638 effective from the latent period for laboratory specimens. However, the electrical
639 resistivity could be difficult to use for damaged structures due to its sensitivity to other
640 parameters [34]. Water-accessible porosity and chloride migration tests are not
641 suitable for the detection of the pathology, their sensitivity being too low with respect
642 to the presence of cracks through the cementitious matrix.

643 • For a given expansion, the permeability increase of concrete damaged by DEF is
644 greater for concrete containing silica aggregate than for concrete with limestone
645 aggregate.

646 • The mechanical tests show that, despite the filling of the ettringite cracking at the end
647 of expansion, no improvement is observed in the measured properties. Only the
648 measurement of the static moduli allows detection of the pathology during the latent
649 period and shows that the loss of moduli seems to be proportional to the expansion
650 measured in stress free conditions.

651 • Three sustainability indicators seem to allow the detection of pathology in the short
652 term during the latent period: gas permeability, electrical resistivity, and static moduli.

653 • The loss of containment in case of nuclear power plants related to the presence of DEF
654 depends of the nature of the aggregates and occurs for less than 20% of damage.

655 • At the acceleration phase, the potential sustainability of concretes is greatly altered
656 and could lead to the premature appearance of other pathologies.

657 • The presence of limestone aggregates seems to improve the sustainability of concrete
658 subject to DEF.

659 This study was performed on a large quantity of laboratory specimens in stress free swelling
660 and fully saturated conditions. It is necessary to pursue the study to evaluate the influence of a
661 larger volume of concrete, the presence of reinforcement and the presence of a water content
662 gradient in order to detect DEF on existing structures. In the case of nuclear power plants, it is
663 also necessary to develop nondestructive methods related to the properties sensitive to DEF
664 proposed in this study in order to maintain the containment property of concrete. In this
665 context, a test platform for the measurement of DEF sustainability indicators on concrete at
666 structure scale is being developed in the ODOBA (Observatoire de la Durabilité des Ouvrages
667 en Béton Armé) project.

668 **Acknowledgment**

669 The authors thank the Institute of Radioprotection and Nuclear Safety (IRSN) for its financial
670 support.

671 **References**

- 672 [1] Brunetaud X., 2005. Etude de l'influence de différents paramètres et de leurs interactions
673 sur la cinétique et l'amplitude de la réaction sulfatique interne au béton. PhD thesis, Ecole
674 Centrale de Paris.
- 675 [2] Leklou N., Aubert J-E., Escadeillas G., 2013. Influence of various parameters on heat-
676 induced internal sulphate attack. European journal of environmental and civil engineering.
677 Vol. 17:3, p. 141-153. <https://doi.org/10.1080/19648189.2012.755338>.
- 678 [3] Zhang Z., Olek J., Diamond S., 2002. Studies on delayed ettringite formation in heat-
679 cured mortars II. Characteristics of cement that may be susceptible to DEF. Cement and
680 Concrete Research. Vol. 17, p. 1737-1742. [https://doi.org/10.1016/S0008-8846\(02\)00894-3](https://doi.org/10.1016/S0008-8846(02)00894-3).
- 681 [4] Petrov N., 2003. Effets combinés de différents facteurs sur l'expansion des bétons causés
682 par la formation différée de l'ettringite. PhD thesis, Université de Sherbrooke.
- 683 [5] Grattan-Bellew P.E., Beaudoin J.J., Vallée V.G., 1998. Effect of aggregate particle size
684 and composition on expansion of mortar bars due to delayed ettringite formation. Cement and
685 Concrete Research. vol. 28, n° 8, p. 1147-1156. [https://doi.org/10.1016/S0008-8846\(98\)00084-2](https://doi.org/10.1016/S0008-8846(98)00084-2).
- 687 [6] Fu Y., Ding J., Beaudoin J. J., 1997. Expansion of Portland cement mortar due to internal
688 sulfate attack. Cement and Concrete Research. Vol. 27, p. 1299-1306.
689 [https://doi.org/10.1016/S0008-8846\(97\)00133-6](https://doi.org/10.1016/S0008-8846(97)00133-6).

- 690 [7] Graf L., 2007. Effect of Relative Humidity on Expansion and Microstructure of Heat-
691 Cured Mortars. RD139. Portland Cement Association. Skokie, Illinois. 50 pages.
- 692 [8] Al Shamaa M., 2012. Etude du risque de développement d'une réaction sulfatique interne
693 et de ses conséquences dans les bétons de structure des ouvrages nucléaires. PhD thesis,
694 Université Paris-Est.
- 695 [9] Kchakech B., 2016. Etude de l'influence de l'échauffement subi par un béton sur le risque
696 d'expansions associées à la réaction sulfatique interne. PhD thesis, Université Paris-Est.
- 697 [10] Al Shamaa M., Lavaud S., Divet L., Nahas G., Torrenti J.-M., 2014. Coupling between
698 mechanical and transfer properties and expansion due to DEF in a concrete of a nuclear power
699 plant. Nuclear Engineering and Design. Vol. 266, p. 70-77.
700 <https://doi.org/10.1016/j.nucengdes.2013.10.014>.
- 701 [11] Jabbour J., 2018. Méthodes d'essais de vieillissement accéléré des bétons à l'échelle des
702 ouvrages. PhD thesis, Université Paris-Saclay.
- 703 [12] NF P18-400, 1981. Bétons - Moules pour éprouvettes cylindriques et prismatiques.
- 704 [13] NF P18-404, 1981. Bétons - Essais d'étude, de convenance et de contrôle - Confection et
705 conservation des éprouvettes.
- 706 [14] Méthode d'essai n°66, 2007. Réactivité d'un béton vis-à-vis d'une réaction sulfatique
707 interne. Laboratoire Central des Ponts et Chaussées.
- 708 [15] PerfDuB, 2017. Determination of the resistivity of saturated concrete.
- 709 [16] XP P 18-461, Testing hardened concrete — Non-steady state chloride migration test –
710 Determination of effective chloride migration coefficient
- 711 [17] XP P18-463, 2011. Bétons - Essai de perméabilité aux gaz sur béton durci.
- 712 [18] NF P18-549, 2010. Béton - Essai pour béton durci - Essai de porosité et de masse
713 volumique.
- 714 [19] NF EN 12390-3, 2003. Essais pour béton durci - Partie 3: résistance à la compression des
715 éprouvettes.
- 716 [20] NF EN 12390-13, 2014. Essai pour béton durci - Partie 13: détermination du module
717 sécant d'élasticité en compression.

- 718 [21] Al Shamaa M., Lavaud S., Divet L., Colliat J.-B., Nahas G., Torrenti J.-M., 2016.
719 Influence of limestone filler and of the size of the aggregates on DEF. *Cement and Concrete*
720 *Composites*. Vol 71, p. 175-180. <https://doi.org/10.1016/j.cemconcomp.2016.05.007>
- 721 [22] Bentz D., Ardani A., Barrett T., Jones S., Lootens D., Peltz M., Sato T., Stutzman P.,
722 Tanesi J. and Weiss J., 2015. Multi-scale investigation of the performance of limestone in
723 concrete. *Construction and Building Materials*. Vol. 75, p. 1-10.
724 <http://dx.doi.org/10.1016/j.conbuildmat.2014.10.042>.
- 725 [23] Yang R., Lawrence C. D., Sharp J.H., 1999. Effect of type of aggregate on delayed
726 ettringite formation. *Advances in Cement Research*. Vol. 11, n°3, p. 119-132.
727 <https://doi.org/10.1680/adcr.1999.11.3.119>.
- 728 [24] Tosun K. and Baradan B., 2010. Effect of ettringite morphology on DEF-related
729 expansion. *Cement and Concrete Composites*. Vol. 32, p. 271-280.
730 <https://doi.org/10.1016/j.cemconcomp.2010.01.002>.
- 731 [25] Bouzabata H., Multon S., Sellier A., Houari H., 2012. Effects of restraint on expansion
732 due to delayed ettringite formation. *Cement and Concrete Research*. Vol. 42, p. 1024–1031.
733 <https://doi.org/10.1016/j.cemconres.2012.04.001>.
- 734 [26] Sagüés A.A., Moreno E.I., and Andrade C., 1997. Evolution of pH during in-situ
735 leaching in small concrete cavities. *Cement and Concrete Research*. Vol. 27, n° 11, p. 1747-
736 1759. [https://doi.org/10.1016/S0008-8846\(97\)00177-4](https://doi.org/10.1016/S0008-8846(97)00177-4).
- 737 [27] Chappex T., and Scrivener K., 2012. Alkali fixation of C–S–H in blended cement pastes
738 and its relation to alkali silica reaction. *Cement and Concrete Research*. Vol. 42, p.1049-1054.
739 <https://doi.org/10.1016/j.cemconres.2012.03.010>.
- 740 [28] Thibaut Y., 2018. Evaluation des structures en béton armé atteintes de réaction sulfatique
741 interne. PhD thesis, Université Toulouse 3.
- 742 [29] Gallucci. E., Zhang. X. and Scrivener. K. L., (2013). Effect of temperature on the
743 microstructure of calcium silicate hydrate (C-S-H). *Cement and Concrete Research*. Vol. 53,
744 p. 185-195. <https://doi.org/10.1016/j.cemconres.2013.06.008>.
- 745 [30] Cagnon. H., Vidal. T., Sellier. A., Bourbon. X. and Camps, G., 2015. Drying creep in
746 cyclic humidity conditions. *Cement and Concrete Research*. vol. 76, p. 91-97.
747 <https://doi.org/10.1016/j.cemconres.2015.05.015>.

- 748 [31] Al Shamaa M., Lavaud S., Divet L., Nahas G., Torrenti J.-M., 2015. Influence of
749 relative humidity on delayed ettringite formation. *Cement and Concrete Composites*. Vol. 58,
750 p. 14-22. <https://doi.org/10.1016/j.cemconcomp.2014.12.013>.
- 751 [32] Brunetaud X., Divet L., Damidot D., 2008. Impact of unrestrained Delayed Ettringite
752 Formation-induced expansion on concrete mechanical properties. *Cement and Concrete*
753 *Research*. Vol. 38, p. 1343–1348. <https://doi.org/10.1016/j.cemconres.2008.05.005>.
- 754 [33] Pavoine A., Brunetaud X., Divet L., 2012. The impact of cement parameters on Delayed
755 Ettringite Formation. *Cement and Concrete Composites*. Vol. 34, p. 521-528.
756 <https://doi.org/10.1016/j.cemconcomp.2011.11.012>
- 757 [34] Rivard P., Saint-Pierre F., 2009. Assessing alkali-silica reaction damage to concrete with
758 non-destructive methods: From the lab to the field. *Construction and Building Materials*. Vol.
759 23, p. 902–909. <https://doi.org/10.1016/j.conbuildmat.2008.04.013>.
- 760 [35] Martin R.-P., Sanchez L., Fournier B., Toutlemonde F., 2017. Evaluation of different
761 techniques for the diagnosis & prognosis of Internal Swelling Reaction (ISR) mechanisms in
762 concrete. *Construction and Building Materials*. Vol. 156, p. 956–964.
763 <https://doi.org/10.1016/j.conbuildmat.2017.09.047>.
- 764 [36] Baroghel-Bouny V. et al., 2004. Conception des bétons pour une durée de vie donnée des
765 ouvrages. Maîtrise de la durabilité vis-à-vis de la corrosion des armatures et de l'alcali-
766 réaction. Etat de l'art et guide pour la mise en œuvre d'une approche performantielle et
767 prédictive sur la base d'indicateurs de durabilité. Guide AFGC.